Structure & Expression, ISBN 0-940030-24-1
Volume 1: From Proteins to Ribosomes, ISBN 0-940030-21-7
Eds., R. H. Sarma & M. H. Sarma, Adenine Press, ©*Adenine Press 1988*

New Aspects in Three-Dimensional Structure Determination of Ribosomal Particles

A.Yonath[1,2] and H. G. Wittmann[3]
[1]Department of Structural Chemistry
Weizmann Institue of Science
Rehovot, Israel

[2]Max-Planck Research Unit for Structural Molecular Biology
Hamburg, FRG

[3]Max-Planck Institute for Molecular Genetics
W. Berlin (Dahlem), FRG

Introduction

The translation of genetic information into a polypeptide chain occurs in a similar manner on ribosomes of all organisms. Ribosomes consist of two different subunits which associate upon initiation of protein biosynthesis. Each subunit is a defined assembly of proteins and ribonucleic acid chains. During the last two decades a vast amount of information has been accumulated about the function and the chemical, biological and genetic properties of ribosomes (1-4). This has shed light on the process of protein biosynthesis, though the understanding of the detailed mechanism is still severely limited by the lack of a molecular model. To this end, we undertook diffraction studies.

As object for crystallographic studies, ribosomal particles are of enormous size, with no internal symmetry. Furthermore, they are instable and flexible. In spite of this, as a result of an intensive systematic exploration of crystallization conditions and development of an innovative experimental technique for fine control of the volume of the crystallization drop (5), procedures for *in vitro* growth of crystals of intact ribosomal particles have been developed. These procedures proved to be suitable for the reproducible production of ordered three-dimensional crystals and two-dimensional sheets of whole 70S ribosomes (6, 7) as well as of their large (50S) ribosomal subunits (8-17). A list which represents the current status is given in Table I.

For all crystallized systems there is a strong correlation between crystallizability and biological activity. Inactive ribosomal particles cannot be crystallized. Moreover, in all cases, the crystalline material retains its biological activity for long

Table I
Packing parameters of two- and three-dimensional crystals of ribosomal particules

Source	Crystal Form	Cell Dimensions, (Å) determined by electron microscopy	X-ray crystallography
70S E.coli	A*	340×340×590; 120°; P6	
70S *Bacillus stearothermophilus*	2D**,AS*	200×440; 93°	
50S *Halobacterium marismortui*	1, P*	310×350; 105°	
	2, P	148×186; 95°	147×181; 97°
	3, P	170×180; 75°	214×300×590; $C222_1$
50S *Bacillus stearothermophilus*	1, A	130×254; 95°	
	2, A	156×288; 97°	
	3, A	260×288; 105°	
	4, A	405×405×256; 120°	
	5, A	213×235×315; 120°	
	6***, A	330×670×850; 90°	360×680×920; $P2_12_12_1$
	2D, A	145×311; 108°; P2	
	2D, AS*	148×360; 109°; P1	

*Crystals are grown by vapor diffusion from alcohols or their mixtures (A), polyethylene glycol (P), or by mixing with ammonium sulphate (AS).
**All forms, unless marked 2D are three-dimensional crystals. 2D = two dimensional sheets.
***Same form and parameters for crystals of the large ribosomal subunits of -L11 mutant of the same source.

periods, in spite of the natural tendency of ribosomes to disintegrate and in contrast to the short life time of isolated ribosomes in solution. Preservation of activity in the crystalline state accords well with the hypothesis that when external conditions (e.g. a cold shock, hibernation, etc.) demand prolonged storage of potentially active ribosomes in living organisms, temporary periodic organization occurs *in vivo*. Currently, three-dimensional crystals and two-dimensional sheets grow from virtually all preparations of active large (50S) ribosomal subunits of *Bacillus stearothermophilus* and of *Halobacterium marismortui*. However, due to the intricate nature of the particles, the exact conditions for the growth of well ordered crystals must still be slightly varied for each ribosomal preparation. Moreover, for each crystal form the quality of the crystals depends, in a manner not yet fully characterized, on the procedure used in preparation of the ribosomal subunits and on the bacterial strain.

Crystallographic Studies

Synchrotron radiation provides the most intense, well collimated X-ray beam. It is essential for data collection from crystals of ribosomal particles. This is due to the large unit cell dimensions (Table I), the shape of the crystals, their fragility and their short life times.

The best three-dimensional crystals grown so far are of the 50S ribosomal subunits

from two bacteria: *Bacillus stearothermophilus* and *Halobacterium marismortui*. Bacterial 50S ribosomal subunits are of molecular weight of about 1,600,000 daltons. Their approximate size of 150 × 170 × 180Å was determined by electron microscopy as well as a variety of biophysical methods (for reviews see 1, 3). They are composed of 2 RNA chains, which comprise two thirds of their total weight, and 30-35 different proteins.

The halophilic ribosomal particles, in contrast to ribosomal particles from eubacteria, are stable and active at high salt concentrations. Thus they provide a system for crystallization from salts or non-volatile compounds (15-17). Crystals from this source grow under conditions which mimic, to some extent, the natural environment within the bacteria. For obtaining large and ordered crystals, advantage has been taken of the delicate equilibrium of mono- and divalent ions needed for the growth of halobacteria as well as of the major role played by the Mg^{++} concentration in crystallization of ribosomal particles. It was found earlier that three-dimensional crystals of 50S ribosomal subunits from *Bacillus stearothermophilus* grow in relatively low Mg^{++} concentration, whereas the production of two-dimensional sheets requires a high Mg^{++} concentration, at which growth of three-dimensional crystals is prohibited (14). Similarly, for spontaneous crystal growth of 50S subunits from *Halobacterium marismortui*, the lower the Mg^{++} concentration is, the thicker the crystals are. With these points in mind, a variation of the standard seeding procedure has been developed. Thin crystals of the 50S subunits from *Halobacterium marismortui*, grown spontaneously under the lowest possible Mg^{++} concentration, are transferred to mixtures in which the Mg^{++} concentration is so low that the transferred crystals dissolve, but after several days new crystals can be observed. These are well ordered and 10-20 fold thicker than the original seeds (Figure 1).

Orthorhombic crystals of the 50S subunits from *Halobacterium marismortui* grow as fragile thin plates with a maximum size of 0.6 × 0.6 × 0.2 mm. They diffract to a resolution of 5.5Å, and have relatively small, compactly packed unit cells of a = 214Å, b = 300Å, c = 590Å, in contrast to the "open" structure of the large crystals of *Bacillus stearothermophilus* (Figure 2). Although between −2°C and 4°C up to 15 photographs can be taken from an individual crystal, the high resolution terms appear only on the first 2-3 X-ray diffraction patterns. Hence, under these conditions over 260 crystals were irradiated in order to obtain a complete data set, and X-ray diffraction data were obtained from crystals which were aligned only visually, with a similar algorithm to that applied for rhino virus (18). However, at cryotemperature (i.e. −180°C), irradiated crystals hardly show radiation damage for days. Thus, for the first time, a full data set could be collected from a single crystal (Figure 3).

Because ribosomes from eubacteria fall apart at high salt concentrations, volatile organic solvents have to be used as precipitants. A modified version of the standard hanging drop technique, using glass plates, was developed (5). The crystallization droplets, which contained no precipitant or an extremely small quantity of it, were equilibrated with a reservoir containing the precipitant. Attempts to increase the size of these crystals by a drastic slow down of the crystallization process failed,

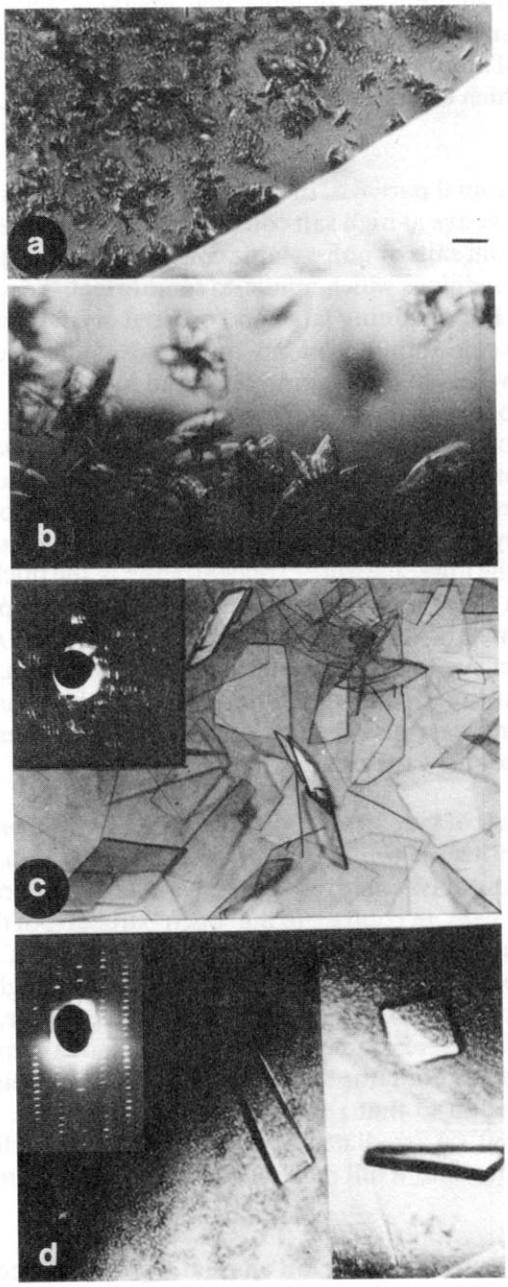

Figure 1: Growth of large, ordered three-dimensional crystals of the 50S ribosomal subunits from *Halobacterium marismortui* by vapor diffusion at 19°C (bar length = 0.2mm). a) Microcrystals obtained within 1-2 days. Droplets of 7-8% polyethylene glycol (PEG), 2.5 M KCl, 0.5 M ammonium chloride, 0.15-0.20 M magnesium chloride and 10 mM spermidine, pH = 5.0-5.2 were equilibrated with 3.0 M KCl, 9% polyethylene glycol, 0.5 M ammonium chloride and 0.20 M magnesium chloride. b) Crystals obtained

within 2-3 days in droplets containing lower KCl concentration than used in (a). Droplet of 4-5% polyethylene glycol, 1.2-1.7 M KCl, 0.5 M ammonium chloride, 0.10 M magnesium chloride and 10 mM spermidine were equilibrated with reservoirs as in (a). c) Crystals obtained within 3-5 days from droplets similar to those used for (b), equilibrated with reservoirs of lower KCl concentrations. Droplet of 4-5% polyethylene glycol, 1.2 M KCl, 0.5 M ammonium chloride, 0.05-0.10 M magnesium chloride and 10 mM spermidine, pH = 5.0-5.6, were equilibrated with 1.7 M KCl, 9% polyethylene glycol, 0.5 M ammonium chloride and 0.10 M magnesium chloride. An X-ray diffraction pattern taken perpendicular to the thin axis of the crystals, obtained under conditions similar to those described in Figure 3, is inserted. d) Crystals obtained by seeding of crystals from (c) in a crystallization drop containing 5% polyethylene glycol, 1.2 M KCl, 0.5 ammonium chloride, 0.03 M magnesium chloride, at pH = 5.6, which was equilibrated with 7% PEG, 1.7 M KCl, 0.5 M ammonium chloride and 0.03 M magnesium chloride, pH = 5.6. Seeds were small, well-shaped crystals, transferred into a stabilization solution of 7% polyethylene glycol in 1.7 M KCl, 0.5 M ammonium chloride, and 0.05 M magnesium chloride at pH = 5.6. An X-ray diffraction pattern taken perpendicular to the thin axis of the crystals, obtained under conditions described in Figure 3, is inserted.

since ribosomal particles from this source are unstable, and may deteriorate before they are able to aggregate and form proper nucleation centers (19).

Growing crystals from volatile organic solvents imposes many technical difficulties in manipulating, data collection and heavy-atom derivatization. In fact, any handling of the crystals, such as removing or reorienting the crystals, or replacing the growth medium by a different solution, is extremely difficult. Thus, for this system seeding was virtually impossible. However, reducing the size of the exposed surface of the crystallizing droplet led to the production of large crystals. This was achieved by growing crystals directly in X-ray capillaries (Figure 2).

Currently crystals from the 50S subunits of wild-type and mutated *Bacillus stearothermophilus* which may reach length of 2.0 mm and a cross-section of 0.4 mm (Figure 2) are obtained at 4°C from mixtures of methanol and ethylene glycol (10 - 13). Since most of the crystals grow with one of their faces adhering to the walls of the capillaries, it is possible to irradiate them without removing the original growth solution. Although most of the crystals grow with their long axes parallel to the capillary axis, a fair number grow in different directions. Thus, it was possible to determine the unit cell constants (Table I) and to obtain diffraction patterns from all of the zones without manipulating the crystals (Figure 2). The crystals are loosely packed (Table I, Figure 2) in a unit cell of 360 × 680 × 920Å. They diffract to 13Å resolution at best (typically 15-18Å). Although they often last a few hours in the synchrotron beam, the higher resolution terms are lost within 5-10 minutes, as in the case of the crystals from the ribosomal particles from the halobacteria.

Oriented arcs and distinct spots, extending to 3.5Å, with spacings similar to those measured from diffuse diffraction patterns of ribosome gels and extracted rRNA (20-22) have been detected on several diffraction patterns of single crystals as well as on those samples containing large numbers of microcrystals. For aligned crystals the average arc length is ± 30°. Such patterns may arise from partial orientation of the nucleic acid component within the particle.

Most recently we were able to obtain three-dimensional crystals from small (30S) ribosomal subunits from *Thermus thermophilus*. These have been grown at 4°C in X-ray

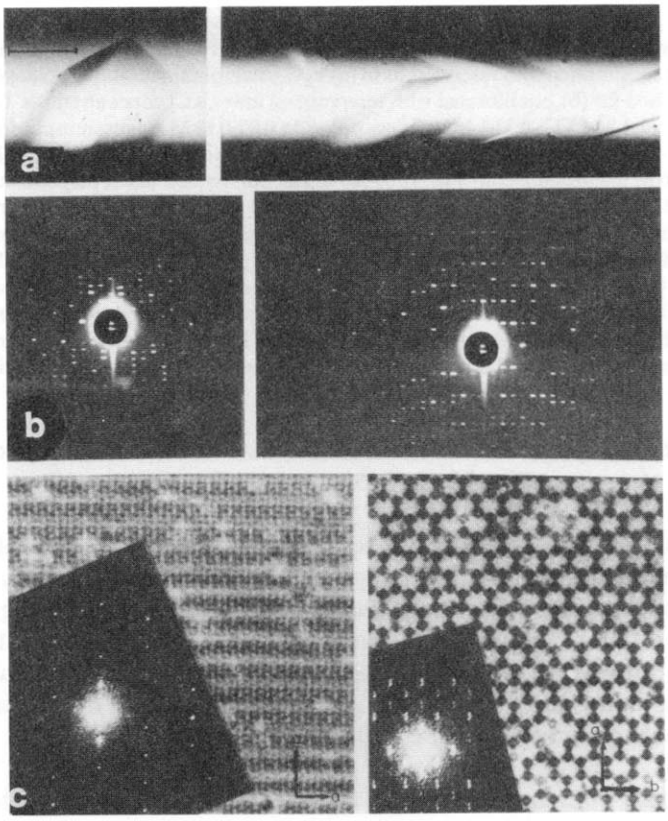

Figure 2: (a) Crystals of the 50S ribosomal subunits from *B. stearothermophilus* grown in 0.5 mm X-ray capillaries by vapor diffusion at 4°C. Crystallization mixture of 20 microliters 50S ribosomal subunits (10-20 mg/ml) in H-I buffer (8), 0.01 M spermine, 1% methanol, 10 mM Hepes or glycine buffer, pH 8.4, was equilibrated with a reservoir of 12% methanol, 12% ethylene glycol, 0.5 M NaCl, pH 8.4.(b) X-ray diffraction patterns from crystals similar to those shown in (a), obtained at −4°C with synchrotron radiation (A1 station at CHESS/CORNELL Univ. operating at 5 GeV, current 30-40 mA) with 0.3 mm collimated X-ray beam with wave length of 1.55Å, on a HUBER precession camera equipped with a He path. Exposure time 3 min, crystal to film distance 200 mm. Left, 1° rotation photograph of 0kl zone, 680 × 920Å. Right, 0.4° rotation photograph of hk0 zone, 360 × 680Å. (c) Electron micrographs of positively stained (2% uranyl acetate) thin sections of crystals similar to those shown in (a) that have been fixed in 0.2% glutaraldehyde and embedded in resin ERL 4206. Optical diffraction patterns are inserted. Left: Section approximately perpendicular to that shown on the right. Repeat distances measured from optical diffraction: 330 × 1050Å. This corresponds to the h0l zone (360 × 920Å) in the X-ray patterns. Right: Micrograph showing the characteristic open packing of this crystal form. The orthogonal choice of axes corresponds to the 680 × 920Å zone observed in the X-ray diffraction patterns. Lattice spacing calculated from optical diffraction: 670 × 850Å.

capillaries, as described in (5), using a mixture of ethylbutanol and ethanol at pH=8.3. Characterization of the crystal is currently underway.

The process of crystal growth is initiated by nucleation. Although many biological molecules and complexes have been crystallized, currently little is known about the mechanism of nucleation. Theoretical models have been developed for the nucleation

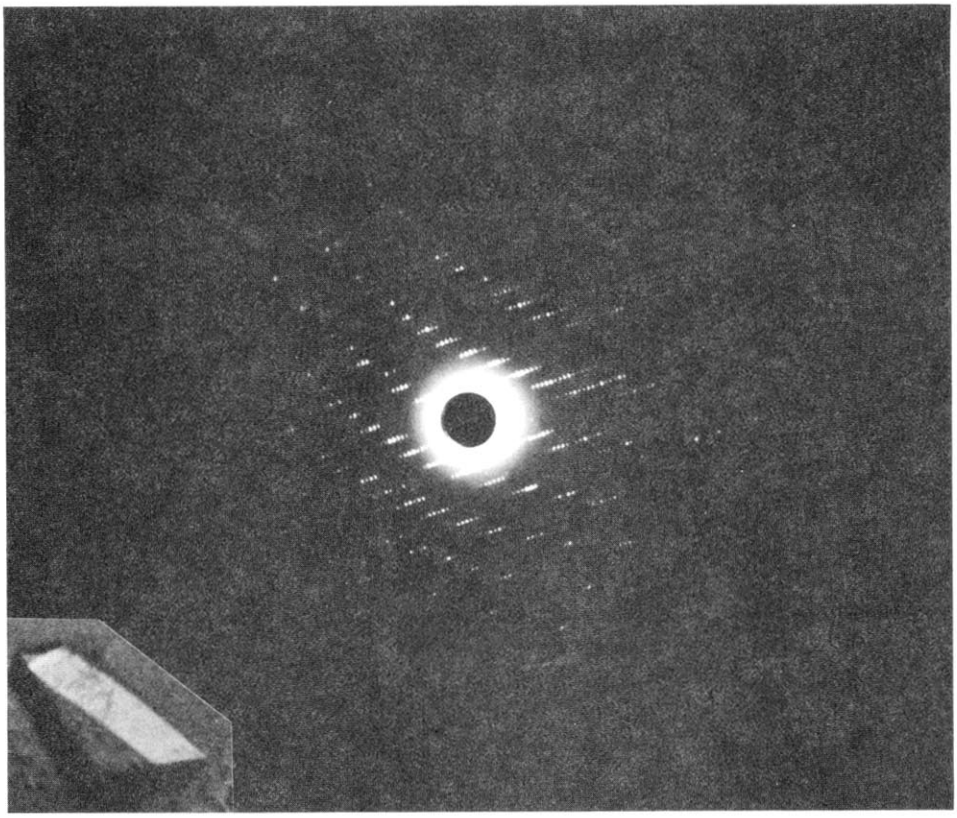

Figure 3: 1° rotation pattern of a crystal similar to the inserted one. The pattern was obtained at −180°C with synchrotron radiation (7.1 station at SSRL/Stanford U. Wave length 1.54Å. Exposure time = 2 min. Crystal to film distance = 135 mm. Insert: A crystal grown under the condition of Figure 1 (d).

of crystals of small molecules (23-24). However, most of the data available concerning the process of nucleation of crystals of biological systems are based on rather indirect evidence, such as monitoring aggregation under crystallization conditions by scattering techniques (25). Because ribosomal particles are large enough to be detected by electron microscopy, crystals of ribosomal particles provide an excellent system for direct investigation of nucleation. The crystallization process was interrupted before the formation of mature crystals, and the crystallization medium was examined by electron microscopy. It was found that the first step in crystal growth is unspecific aggregation and that nucleation starts by a rearrangement within the aggregates (19).

Phase Determination

The most common method in protein crystallography to derive phases is multiple isomorphous replacement (MIR). For an object as large as the 50S ribosomal subunit, it is necessary to use extremely dense and compact compounds as heavy atom derivatives. Examples for this purpose are tetrakis(acetoxy-mercuri)methane which

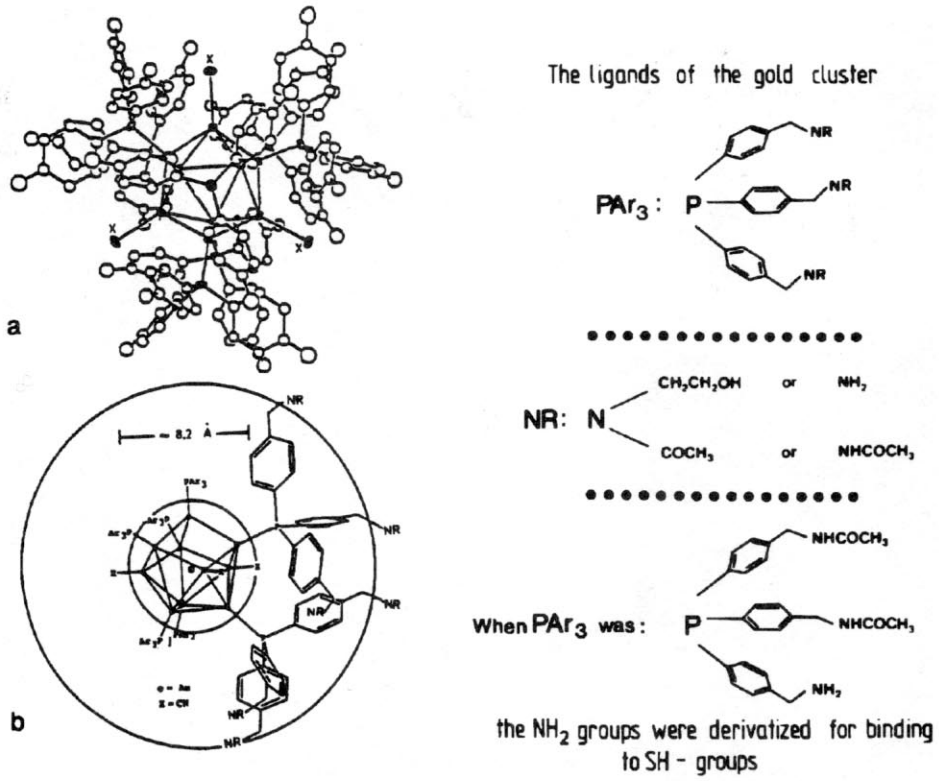

Figure 4: (a) Postulated molecular structure of the gold cluster used by us based on the crystal structure of a similar cluster (48). (b) Semi-schematic presentation of the gold cluster depicting the gold core of 8.2Å diameter, and the arrangement of the ligands around it (49).

was the key heavy atom derivative in the structure determination of nucleosomes and the membrane reaction center (26,27), and an undecagold cluster, in which the gold core has a diameter of 8.5Å (Figure 4). Several variations of this cluster, prepared with different ligands have been prepared in an equilibrium mixture (S. Weinstein and W. Jahn, in preparation). Some variants are soluble in the crystallization solution of 50S subunits from *H. marismortui*. One of these variants, in which all the NR moieties are amines, was used for the formation of a heavy-atom derivative by soaking of native crystals in its solution. Crystallographic data (to 18Å resolution) show isomorphous unit cell constants with observable differences in the intensities.

Because the surface of the ribosomal subunit is a composite of a variety of potential binding sites for such clusters, in parallel to soaking experiments attempts to bind the heavy-atom derivatives covalently to a few specific sites on the ribosomal particles are in progress. This may be achieved either by direct interaction of a heavy-atom cluster with chemically active groups such as -SH or the ends of rRNA (28) on the intact particles prior to crystallization or by covalent attachment of a cluster to tailor-made carriers which bind to one or a few specific sites on ribosomes.

To this end, the following approaches were taken: Firstly, free sulfhydryls on the surface of the 50S subunit have been located by reacting with radioactive N-ethylmaleimide. The binding sites were analyzed by locating radioactivity in two-dimensional gels of the ribosomal proteins. It was found that in the case of 50S subunits from *B. stearothermophilus* there are two proteins (L11 and L13) which definitely bind N-ethylmaleimide. For *H. marismortui* a significant portion of the radioactivity was associated with one protein. Secondly, the gold cluster described above was prepared such that it could be bound to accessible -SH groups. Since this cluster is rather bulky, its accessibility was increased by the insertion of spacers, differing in length, to the cluster as well as to the free -SH groups on the ribosomal particles. Radioactive labelling of this cluster as well as neutron activation analysis enabled us to determine the extent of the association of the cluster with the particles. The results of both analytical methods show that a spacer of minimum length of about 10Å between the -SH group of a ribosomal protein and the N-atom on the cluster, is needed for significant binding. Furthermore, the extent of binding depends also on the structure of the spacer (S. Weinstein and W. Jahn, in preparation). Preliminary experiments indicate that the products of the derivatization reaction with 50S particles could be crystallized.

As mentioned above, such clusters may also be bound to biochemical carriers. Examples for these are antibiotics (29), DNA oligomers complementary to exposed single-stranded rRNA regions (30) and Fab molecules specific to ribosomal proteins. Since most of the interactions of these materials are characterized biochemically, the crystallographic location of the heavy-atom compounds will not only be used for phase determination but will also reveal the location of specific sites on the ribosome.

Alternatively, such clusters may be attached to chosen sites on isolated ribosomal components which will subsequently be incorporated into particles in which they are missing. A mutant of *Bacillus stearothermophilus* which lacks protein L11 was obtained by growing cells in the presence of thiostrepton at 60°C (31). The 50S mutated ribosomal subunits crystallize in two and three dimensions under the same conditions as, and are isomorphous to, those obtained from the 50S ribosomal subunits of the wild type (12). This shows that L11, the missing protein, is not involved in crystal forces in the native crystals. Furthermore, protein L11 has only one sulfhydryl group, and binding of N-ethylmaleimide to it does not reduce the activity and crystallizability of the reconstituted modified particles.

Since protein L11 is believed to be nearly globular (32), its location may be determined in a Patterson vector density map with coefficients of F(wild)-F(mutant), and may serve, by itself, as a super large heavy-atom derivative. At preliminary stages of structure determination this approach may provide phase information and reveal the location of the missing protein.

Three-Dimensional Image Reconstruction

The large size of ribosomal particles, which is an obstacle for crystallographic

studies, permits direct investigation by electron microscopy. Electron microscopy of crystalline ribosomal arrays can be used to locate and orient the particles within the crystals. A model obtained by three-dimensional image reconstruction of two-dimensional sheets may be used for gradual phasing of low resolution crystallographic data. These phases, in turn, may help to locate heavy atom sites for the isomorphous replacement technique. To this end, we have initiated three-dimensional image reconstruction studies.

Most of the two-dimensional sheets from prokaryotic ribosomal subunits have been grown *in vitro* from low molecular weight alcohols (AL) by vapor diffusion in hanging drops (14, 33). Recently, mixtures of salts and alcohols (ST) have been used for the growth of two-dimensional sheets in depression slides or on electron-microscopy grids (7, 14, 34-37). Well ordered two-dimensional sheets from the 70S ribosomes and from 50S subunits from *Bacillus stearothermophilus* have been subjected to three-dimensional image reconstruction studies at 47Å and 30Å resolution (34,37), respectively. In both cases the reconstructed particles have average dimensions similar to those determined by other physical methods (3). Moreover, on the basis of the known molecular weight of the 70S and 50S particle (2.300.000 and 1.600.000 daltons, respectively) and of the volume obtained from the three-dimensional image reconstruction, the calculated densities are in good agreement with values tabulated (38) and calculated for the crystals of the 50S subunits from *H. marismortui* (17) and other nucleoproteins (39-41).

The two-dimensional sheets of 70S particles from *Bacillus stearothermophilus* are built of dimers, packed in relatively small unit cells: Several features were revealed by the analysis (Figure 5) of the models obtained from gold-thioglucose stained sheets. The two ribosomal subunits are arranged around an empty space, large enough to accomodate most of the components of protein biosynthesis. There are variations in the size of this space as revealed in different reconstructions. This may result from sheets, built of ribosomes which may carry a different number of components of protein biosynthesis, such as tRNAs or fragments of mRNA.

The two ribosomal subunits are fairly well resolved. The overall shapes of both subunits were compared with models previously suggested for these particles. There is a similarity between the model of the small subunit obtained by visualization of single particles (3) and that revealed by our studies. However, isolated 30S particles seem to be shorter and wider than the reconstructed ones within the 70S particles. This may be a consequence of the contact of the isolated particles with the flat electron microscope grid. In contrast, particles within the crystalline sheets are held together by crystalline forces. These construct a network which may stabilize the conformation of the particle and decrease, or even eliminate, the influence of the flatness of the grids. The portion of the reconstructed 70S particle which we assigned as the large subunit, may be correlated to the image of this subunit as revealed (Figure 6, and in (34)) both at 28Å (the actual resolution of the studies) and at 55Å (see below).

Reconstruction of models of 70S ribosomes from sheets stained with uranyl acetate

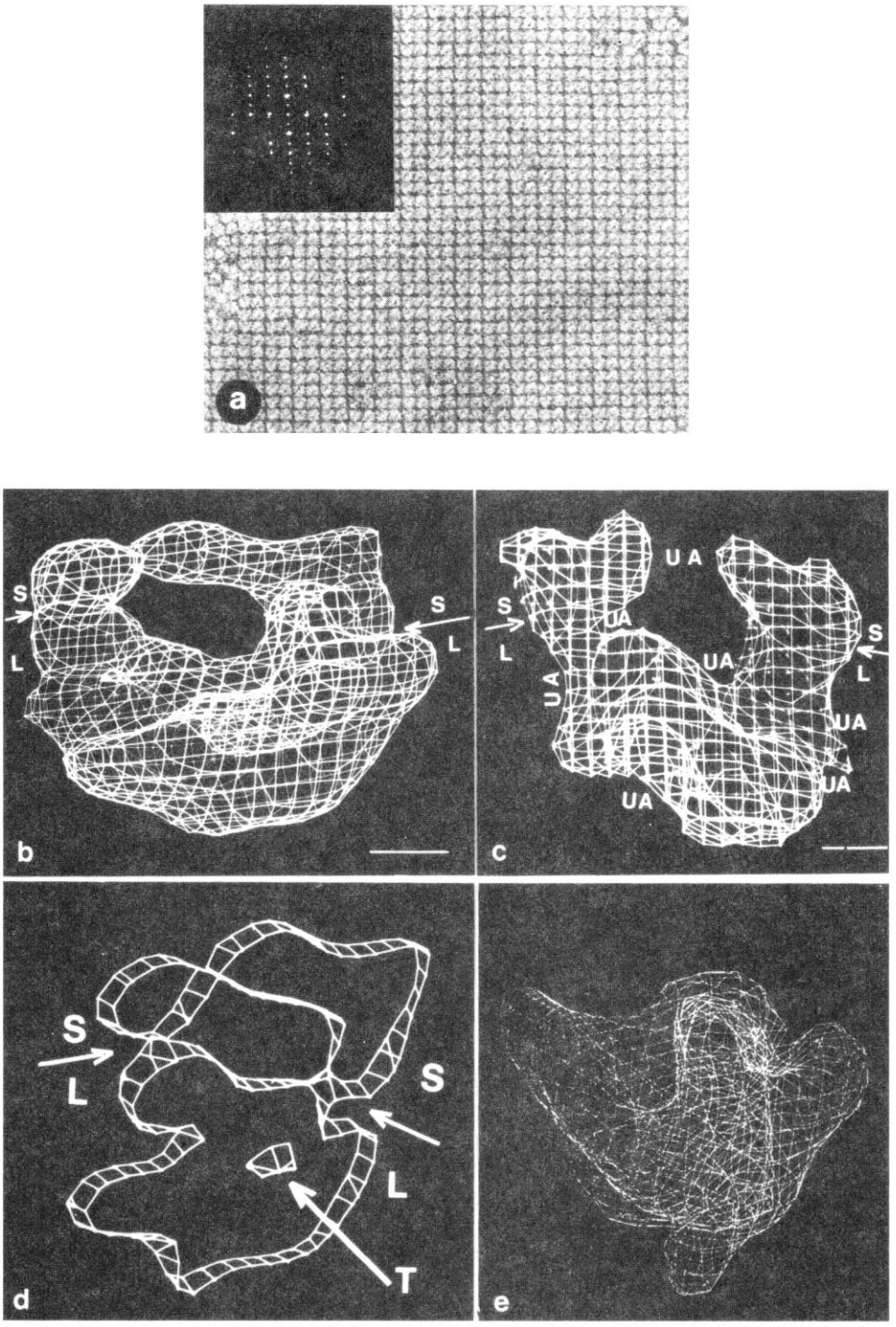

Figure 5: *continued on next page*

Figure 5: Computer graphic display of the outline of the reconstructed model of the 70S ribosome at 47Å resolution. (a) Image of a two-dimensional sheet (×28000) of 70S particles from *B. stearothermophilus*, stained by gold-thioglucose, and an optical diffraction pattern from an area containing about 20×15 unit cells. (b) Computer graphic display of the outline of the reconstructed model of the 70S ribosome at 47Å resolution, stained with gold-thioglucose. L and S indicate the 50S and the 30S subunits, respectively. The arrows point at the interface between the two subunits. Bar length = 20Å. (c) Computer graphic display of the outline of the reconstructed model of the 70S ribosome at 42Å resolution stained with uranyl acetate, at a similar orientation to that shown in (b). UA shows the regions to which uranyl acetate binds. L and S indicate the 50S and the 30S subunits. The arrows point at the interface between the two subunits. Bar length = 20Å. (d) The outline of a 20Å thick section in the middle of the reconstructed model of the 70S ribosome. T indicates part of the tunnel. (e) The 30Å resolution reconstructed model of the 50S subunit, obtained as in Figure 6, viewed in a projection which resembles models derived from electron microscopy studies of single particles.

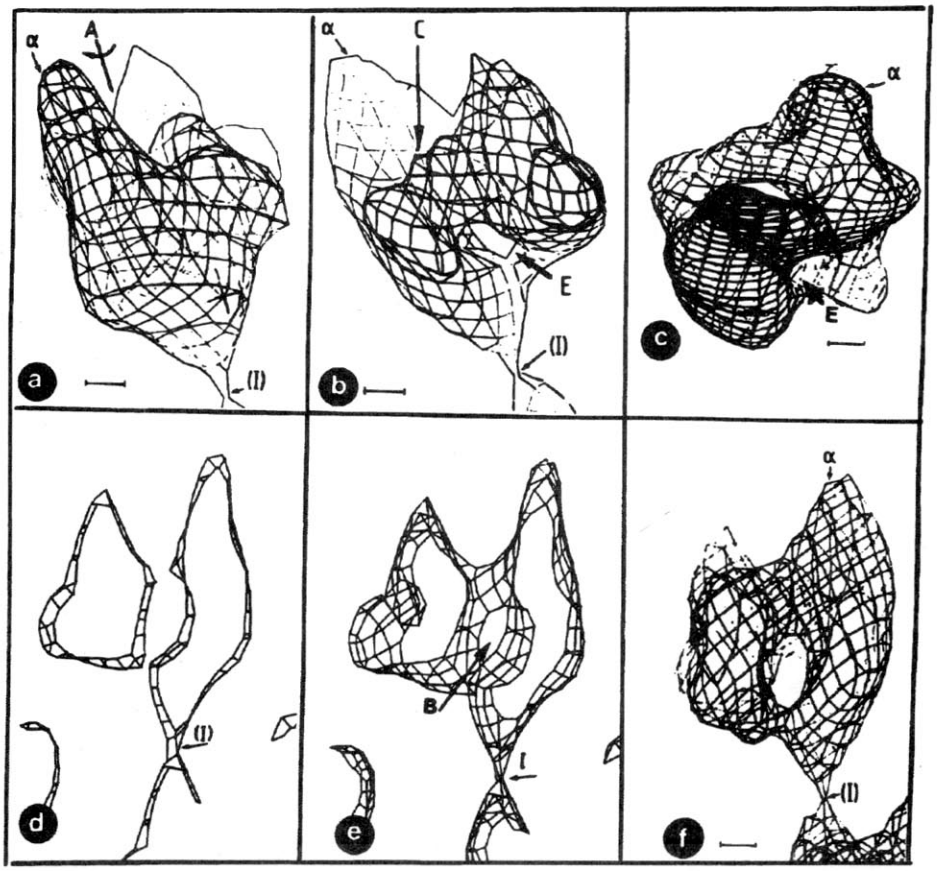

Figure 6: Computer graphic display of the outline of the reconstructed model of the 50S ribosomal subunit at 30Å resolution. α marks the longest arm. (E) is the exit site. (a) A side view of the model. The entire particle and part of a second one are shown. The arrow (I) points at the crystal contact between the two particles. (A) marks the approximate axis around which the model was turned to obtain the view shown in (b). Bar length = 20Å. (b) The model shown in (a) rotated about the (A) axis. (C) points at the cleft between the projecting arms, at the site it turns into the tunnel. (c) A view into the tunnel from the cleft. (d) The outline of a 20Å thick section in the middle of the reconstructed model, showing that the tunnel spans the particle. (e) The outline of a 40Å thick section in the middle of the reconstructed model. The branching of the tunnel is seen (B). (f) The model viewed into the branch of the tunnel from the exit point.

led to a model which shows the features described above, as well as regions where uranyl acetate, acting as a positive stain, was incorporated into the particle. This may indicate that in these regions the RNA is concentrated and/or easily exposed to the stain. Such regions are located on the surface of the large subunit where it faces the internal empty space. Penetration of uranyl acetate to the region assigned as "collar's ridge" on the small subunits was also detected. In both cases the staining of these areas with uranyl acetate may stem either from the existence of exposed rRNA regions, as previously found (42), or from the presence of mRNA and tRNA in these locations.

The two-dimensional sheets of the 50S subunits consist of small unit cells: $145 \pm 3 \times 311 \pm 14$ Å, gamma = $89 \pm 2.6°$ for the alcohol grown arrays, and $148 \pm 10 \times 370 \pm 20$ Å, gamma = $109 \pm 3°$ for those grown from salts. These cell dimensions are close to those of forms 1 and 2 of the three-dimensional crystals from the same source (43 and Table I). Both (AL) and (ST) sheets are well ordered, and optical diffraction patterns of electron micrographs of negatively stained specimens with gold-thioglucose extend to 30 Å and 28 Å, respectively.

Interparticle contacts within particles in the sheets are clearly revealed in the resulting three-dimensional map. The best defined contact area is of about 10-15Å diameter, compatible with the regular intermolecular contacts found in crystals of proteins or nucleic acids. As details as small as these are beyond the resolution of our map, we cannot yet identify the nature of these contacts.

Several striking features have been revealed in the resulting model (Figure 6). The concave surface of the particle consists of several protrusions of 25-30Å diameter, the approximate size of globular proteins of molecular weights typical of many ribosomal proteins. Several projecting arms, two of which are longer than the others, are arranged radially around the edge (upper side of the particle shown in Figure 6), near the presumed interface with the 30S subunit. A narrow elongated cleft is formed between the projecting arms and turns into a tunnel of a diameter of up to 25Å and 100-120Å length. Another long arm is located on the other side of the particle (bottom of the particle shown in Figure 6).

Thirteen reconstructed particles were studied. The tunnel is present in all reconstructions of the (ST) sheets independent of the staining material. Furthermore, indications of such a tunnel are detected in some filtered images of particular tilts (Figure 7). In every reconstructed particle there is a region of low density which branches off the tunnel to form a Y (or V) shape and terminates on the opposite side of the particle (Figure 6). As yet the exact nature of this region cannot be determined. It may be a loosely packed protein region, but in some reconstructed models the density of this region is so low that it appears as a branch of the main tunnel.

Three-dimensional image reconstruction was applied to two-dimensional sheets stained with uranyl acetate, too. Although the arrays used were large and well ordered, the diffraction patterns of their micrographs extended only to 32Å, and were of lower quality than those from gold-thioglucose. This might stem from the

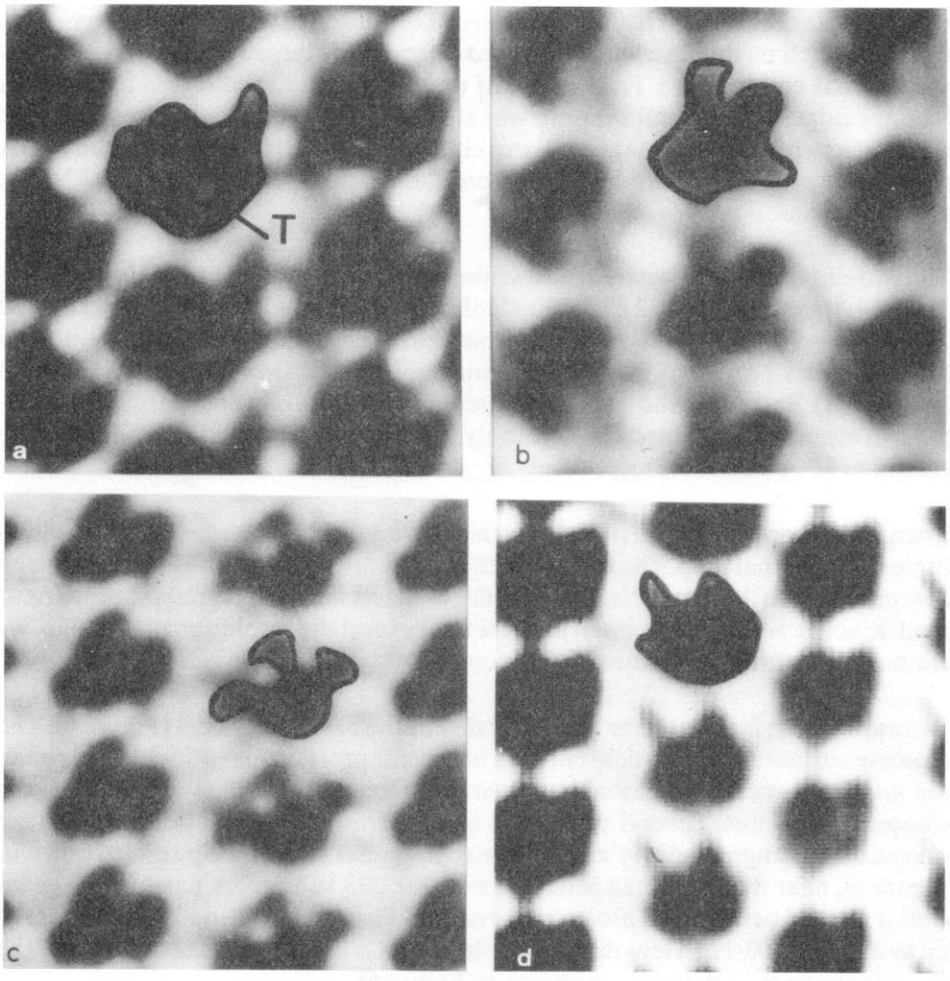

Figure 7: Filtered images of electron micrographs of sheets of 50S subunits from *B. stearothermophilus* in which the depicted view resembles that derived from electron microscopy of single particles. (a) (AL) sheets stained with uranyl-acetate. Tilt angle of 25°. (b-d) (ST) sheets stained with gold-thioglucose. In (b) and (d) "conventional views" can be seen (tilts of 35° and 20°, respectively). The tunnel T can be detected in (a).

fact that uranyl acetate is not a pure negative stain and may interact with selected parts of the particle (presumably the rRNA). This interaction may depend on the accessibility to the stain and therefore be somewhat irregular. Consequently, the reconstructed model shows less details. For the (ST) sheets, the essential features - the concave shape, the tunnel and the projecting arms - are resolved.

Comparison of this model with that obtained from the same crystals (ST) stained with gold-thioglucose shows three regions (on one of the long arms, and on the body

of the particle and near the subunit interface) where uranyl acetate, acting as a positive stain, is incorporated into the particle. This may indicate that in these regions the rRNA is concentrated and/or easily exposed to the stain.

Several models for the 50S ribosomal subunits from *E. coli* have been suggested previously based on electron microscopical visualization, reconstruction or averaging of single particles. Our model can be positioned so that its projected view resembles the usual image seen when single particles are investigated by electron microscopy (Figure 5). In addition, there are a few filtered images of two-dimensional sheets tilted by certain angles, which show the same shape and include the characteristic features that have been visualized by electron microscopy of single particles (Figure 7). At the same time there are, however, major discrepancies in the nature of the gross structural features between our model and the others, which, as in the case of the 70S particles stem from the basic differences between visualization of isolated particles in projection and the inherently more objective character of structure analysis by diffraction methods.

In order to understand why some of the features revealed in our studies have not yet been detected in previous investigations, we have reconstructed a model selecting from the entire set of diffraction data only the low resolution (55Å) terms. In spite of the low resolution the tunnel is clearly resolved. However, at this resolution the particle is almost spherical and shows only two thick and short arms instead of the elongated ones resolved in the high resolution studies. It should be mentioned that the tunnel is clearly resolved at this resolution. Furthermore, a similar feature, a narrow elongated region of low density was also detected on ribosomes from chick embryos by three-dimensional image reconstruction (42). However, in the 70S reconstructed particle there are only some indications for the existence of a tunnel. Thus, a portion of the tunnel could be detected in a section through the particle (Figure 5). As mentioned above the 70S particles were harvested while being active and it is feasible that nascent protein chains are still attached to a part of them. It is conceivable that the tunnel is only partially resolved due to this and/or to the intrinsic low resolution of this reconstruction.

The functional significance of the tunnel is still to be determined. However, originating at the presumed site for actual protein biosynthesis and terminating on the other end of the particle, and being of a diameter large enough to accomodate even the largest amino acids, this tunnel appears to provide the path taken by the nascent polypeptide chain. Furthermore, this tunnel is of a length which could accomodate and protect from proteolytic enzymes, a peptide of about 40 amino acids in an extended conformation (44-46). It remains to be seen whether the tunnel terminates at a location compatible with that assigned by immune electron microscopy as the exit site for the growing polypeptide chain (47).

Concluding Remarks

We have demonstrated here that diffraction methods can be employed for the determination of the three-dimensional structure of intact ribosomal particles. We expect

that our studies, supported by biophysical, biochemical and genetic knowledge, will yield a reliable model for the ribosome and lead to the understanding of the molecular mechanism of protein biosynthesis.

Acknowledgement

We would like to thank Dr.H. Hope for introducing cryo-temperature crystallography; Drs. S. Weinstin and W. Jahn for the preparation and the incorporation of the gold cluster; Drs. M.A. Saper, K.S. Bartels, F. Frolow, C. Kratky and G. Weber for their efforts in data collection; Dr. K.R. Leonard for participation in the image reconstruction studies, Dr. F.L. Hirshfeld for his critical comments: Drs. J. Sussman and B. Shaanan for assisting us with computing and display problems; Dr. M. Shoham for his contribution to the crystallization process; Drs. K. Wilson, H.D. Bartunik, J. Helliwell, M. Papiz, K. Moffat, W. Schildcamp, P. Phizackerley, and E. Merrit in providing us with synchrotron radiation facilities; and I. Makowski, T. Arad, P. Webster, H.S. Gewitz, J. Piefke, J. Müssig, J. Halfon, C. Glotz, B. Romberg, G. Idan and H. Danz for technical assistance. This work was supported by BMFT (05 180 MP BO), NIH (GM 34360) and Minerva research grants.

References and Footnotes

1. G. Chambliss, G.R. Craven, J. Davies, L. Kahan and M. Nomura. eds., *Ribosomes: Structure, Function and Genetics*. Univ. Park Press, Baltimore (1980).
2. H.G. Wittmann, *Annual Rev. Biochem. 51*, 155-187 (1982).
3. H.G. Wittmann, *Annual Rev. Biochem. 52*, 35-65 (1983).
4. B. Hardesty and G. Kramer, eds., in: *Structure, Function and Genetics of Ribosomes*. Springer Verlag, Heidelberg and N.Y. (1986).
5. A. Yonath, J. Müssig and H.G. Wittmann, *J. Cell Biochem. 19*, 145-155 (1982).
6. H.G. Wittmann, J. Müssig, H.S. Gewitz, J. Piefke, H.J. Rheinberger and A. Yonath, *FEBS Letters 146*, 217-220 (1982).
7. J. Piefke, T. Arad, I. Makowski, H.S. Gewitz, B. Hennemann, A. Yonath and H.G. Wittmann, *FEBS Letters 209*, 104-106 (1986).
8. A. Yonath, J. Müssig, B. Tesche, S. Lorenz, V.A. Erdmann and H.G. Wittmann, *Biochem. Inter. 1*, 428-435 (1980).
9. A. Yonath, J. Piefke, J. Müssig, H.S. Gewitz and H.G. Wittmann, *FEBS Letters 163*, 69-78 (1983).
10. A. Yonath, H.D. Bartunik, K.S. Bartels and H.G. Wittmann, *J. Mol. Biol. 177*, 201-206 (1984).
11. A. Yonath, M.A. Saper, I. Makowski, J. Müssig, J. Piefke, H.D. Bartunik, K.S. Bartels and H.G. Wittmann, *J. Mol. Biol. 187*, 633-636 (1986).
12. A. Yonath, M.A. Saper, F. Frolow, I. Makowski and H.G. Wittmann, *J. Mol. Biol. 192*, 161-162 (1986).
13. A. Yonath, M.A. Saper and H.G. Wittmann, in: *Structure, Function and Genetics of Ribosomes* (B. Hardesty and G. Kramer, eds.), Springer Verlag, Heidelberg and N.Y., pp. 112-127 (1986).
14. T. Arad, K.R. Leonard, H.G. Wittmann and A. Yonath, *EMBO J. 3*, 127-131 (1984).
15. A. Shevack, H.S. Gewitz, B. Hennemann, A. Yonath and H.G. Wittmann, *FEBS Letters 184*, 68-71 (1985).
16. M. Shoham, J. Müssig, A. Shevack, T. Arad, H.G. Wittmann and A. Yonath, *FEBS Letters 208*, 321-324 (1986).
17. I. Makowski, F. Frolow, M.A. Saper, H.G. Wittmann and A. Yonath, *J. Mol. Biol. 193*, 819-822 (1987).
18. M.G. Rossmann and W. Erickson, *J. Appl. Cryst. 16*, 629-636 (1983).
19. A. Yonath, G. Khavitch, B. Tesche, J. Müssig, S. Lorenz, V.A. Erdmann and H.G. Wittmann, *Biochem. Inter. 5*, 629-636 (1982).
20. A. Klug, K.C. Holmes and J.T. Finch, *J. Mol. Biol. 3*, 87-100 (1961).

21. G. Zubay and M.H.F. Wilkins, *J. Mol. Biol. 2*, 105-112 (1960).
22. R. Langridge and K.C. Holmes, *J. Mol. Biol. 5*, 611-617 (1962).
23. J.W. Gibbs, in: *Collected Works of J.W. Gibbs*, Longmas Green, N.Y., pp. 55-70 (1928).
24. A.C. Zettelmeyer, in: *Nucleation*, Marcel Dekker, New York (1969).
25. Z. Kam, H.B. Shore and G. Fehder, *J. Mol. Biol. 123*, 539-557 (1978).
26. J. Deisenhofer, O. Epp, K. Mikki, R. Huber and H. Michel, *J. Mol. Biol. 180*, 385-398 (1984).
27. T. Richmond, J.T. Finch, B. Rushton, D. Rhodes and A. Klug, *Nature 311*, 533-535 (1984).
28. O.W. Odom Jr., D.R. Robbins, J. Lynch, D. Dottavio-Martin, G. Kramer and B. Hardesty, *Biochemistry 19*, 5941-5947 (1980).
29. K.H. Nierhaus and H.G. Wittmann, *Naturwissenschaften 67*, 234-288 (1980).
30. W.E. Hill, B.E. Trappich and B. Tassanakajohn, in: *Structure, Function and Genetics of Ribosomes* (B. Hardesty and G. Kramer, eds.), Springer Verlag, Heidelberg and N.Y., 233-252 (1986).
31. J. Schnier, H.S. Gewitz, B. Leighton, in preparation (1986).
32. L. Giri, W.E. Hill, H.G. Wittmann and B. Wittmann-Liebold, *Adv. Prot. Chem. 36*, 1-10 (1984).
33. M.W. Clark, K.R. Leonard and J.A. Lake, *Science 216*, 999-112 (1982).
34. A. Yonath, K.R. Leonard and H.G. Wittmann, *Science 236*, 813-816 (1987).
35. J. Piefke, T. Arad, H.S. Gewitz, A. Yonath and H.G. Wittmann, *FEBS Lett. 209*, 104-107 (1986).
36. T. Arad, J. Piefke, H.S. Gewitz, B. Romberg, C. Glotz, J. Müssig, A. Yonath and H.G. Wittmann, *Anal. Biochem.*, in press (1987).
37. T. Arad, J. Piefke, S. Weinstein, H.S. Gewitz, A. Yonath and H.G. Wittmann, *Biochimie*, in press (1987).
38. B.W. Matthews, *J. Mol. Biol. 33*, 491-497 (1968).
39. J.M. Hogle, *J. Mol. Biol. 160*, 663-668 (1982).
40. L. Liljas, T. Unge, A. Jones, K. Fridborg, S. Lovgren, U. Skoglund and B. Strandberg, *J. Mol. Biol. 159*, 93-108 (1982).
41. J.T. Finch, L.C. Lutter, D. Rhodes, R.S. Brown, B. Rushton, M. Levitt M. and A. Klug, *Nature 269*, 29-32 (1977).
42. R.A. Milligan and P.N.T. Unwin, *Nature 319*, 693-696 (1986).
43. A. Yonath, *TIBS 9*, 227-229 (1984).
44. L.I. Malkin and A. Rich, *J. Mol. Biol. 26*,329-346 (1967).
45. G. Blobel and D.D. Sabatini, *J. Cell. Biol. 45*, 130-145 (1970).
46. W.P. Smith, P.C. Tai and B.D. Davis, *Proc. Natl. Acad. Sci. USA 75*, 5922-5925 (1978).
47. C. Bernabeau and J.A. Lake, *Proc. Nat. Acad. Sci. USA 79*, 3111-3115 (1982).
48. P. Bellon, M. Manassero and M. Sansoni, *J. Chem. Soc. Dalton*, 1481 (1972).
49. J.S. Wall, J.F. Hainfeld, P.A. Barlett and S.J. Singer, *Ultramicroscopy 8*, 397-406 (1982).